JOURNAL OF MATERIALS SCIENCE **39** (2004) 2841–2848

Annealing twin boundary cracking in the low-temperature brittle fracture of a high-nitrogen bearing austenitic steel

SHIYONG LIU*
Institute of Metal & Technology, Dalian Maritime University, Dalian 116026, People's Republic of China
E-mail: shiyong@newmail.dlmu.edu.cn

SHICHENG LIU, DEYI LIU
Department of Materials Science and Engineering, Dalian Railway Institute, Dalian 116028, People's Republic of China

Crack propagation paths in the low temperature brittle fracture of 18Cr-18Mn-0.7N austenitic steel were investigated by means of scanning electron microscopy. Corresponding relationships of the fracture facets with microstructures were established by the simultaneous observation of the fracture surface and the microstructure of the adjacent side surface. It was shown that the annealing twin boundary cracking occurred during fracture. A great deal of twins formed during solution treatment of the steel, with steps several microns high on the twin boundaries, and a considerable amount of planar deformation structures developed on {111} planes in the fracture process. The fracture facets of the annealing twin boundary are fairly flat and smooth, with bent steps of micron-scale height, and a pattern of three sets of parallel straight-lines intersecting at 60°. But there is no river pattern on the facets. The bent steps result from partial propagation of crack along steps that are developed on annealing twin boundaries during solution treatment, while the line-pattern is the intersection traces of the planar deformation structures with the fracture facet. It is believed that the annealing twin boundary cracking is attributed to the stress concentration arising at the intersection of planar deformation structures and the annealing twin boundaries.

1. Introduction

High-nitrogen bearing austenitic steels show attractive features of high strength and excellent stress corrosion cracking resistance without deteriorating toughness at room temperature. With decrease in temperature, however, the steels exhibit clear ductile-to-brittle transition behavior, which is contrary to usual expectations for face-centered cubic (fcc) materials [1–4]. In order to clarify the brittle fracture mechanism at low temperatures, careful fracture examinations were conducted, and flat facets forming along {111} planes were recognized on the fracture surface [1–4]. These flat facets were believed to satisfy the definition of cleavage crack in ASTM's Standard E 616 [5]. To explain the formation of these flat facets, Müllner *et al.* [6] proposed a model which claims that interactions of mechanical twins on different planes cause microcleavage. Tobler *et al.* [1] termed this kind of fracture mechanism slip-band cracking. Tomota *et al.* [2, 4] put forward that fracture took place along {111} planes by slipping-off, i.e., separation occurring along an active slip plane with a high density of dislocations. However, they could not explain why there were no river patterns on the fracture facets, the characteristic feature on cleavage facets in body-centered cubic (bcc) steels [7–9]. For this reason, the flat facets were called transgranular cleavage-like fracture facets in early works [1–4]. It should be seen that the brittle fracture mechanism at low temperatures in this kind of steels remains unknown. The key point of solving the problem is to reveal the essence of the fracture facets mentioned above.

Recently, one of the authors has examined the fracture propagation behavior and the fracture surface at low temperatures in an 18Cr-18Mn-0.7N high-nitrogen bearing austenitic steel and shown that there exists annealing twin boundary cracking in the low temperature brittle fracture of the steel [10]. Careful observations demonstrated that the so called transgranular cleavage-like fracture facets in earlier studies are in effect annealing twin boundary fracture facets. In this study, some additional examinations on the annealing twin boundary fracture facets were conducted in detail, and

*Author to whom all correspondence should be addressed.

a fracture mode has been proposed to explain their formation mechanism.

2. Experimental material and procedure

An 18Cr-18Mn-0.7N high-nitrogen bearing austenitic steel, with the composition of 0.048C, 19.33Cr, 19.40Mn, 0.70N, 0.42Si, 0.029P, 0.008S, 0.27Ni (wt%), and balance Fe, was employed in the present work. The ingot was hot forged and rolled into sheets 2 and 10 mm thick. Then the sheets were heated at 1323 K for 3.6 ks under an Ar gas atmosphere followed by water cooling. Tensile test specimens were machined into bars of 2×5 mm cross section with 30 mm of gage length, and the loading axis was aligned in the rolling direction. Tensile tests were performed at 293, 77 and 4 K respectively at a strain rate of 5.5×10^{-4} s^{-1}. Correspondingly, the total test times were 1044, 185, and 18 s. Charpy impact tests were carried out at temperatures from 77 to 293 K using ASTM standard V-notched Charpy impact test specimens of an L-T orientation prepared according to ASTM E 616 [5]. The dimensions of the Charpy specimens were 55 mm long and 10 mm square. Cracking path, fracture surface and microstructure of the ruptured specimens were examined using scanning electron microscope (SEM). The crystallographic features of deformed structures and fracture facets were analyzed as well.

3. Results and discussion

3.1. Microstructure after solution treatment

Microstructure of the test specimens after solution treatment is single-phase austenite with many annealing twins. Fig. 1 shows the microstructure of a tensile specimen polished and etched after solution treatment. Annealing twins and annealing twin boundaries are obviously shown and there are micron-scale steps on the annealing twin boundaries as exemplified by the arrow in the figure.

3.2. Embrittlement behavior at low temperatures

Stress-strain curves in tensile tests and impact energy-temperature curve of the test steel are shown in Fig. 2.

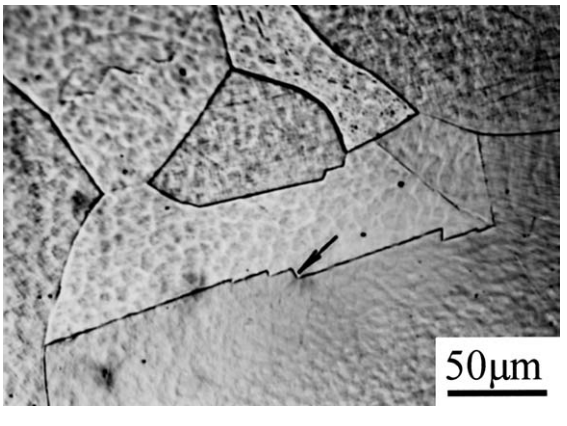

Figure 1 Optical microstructure on the surface of a tensile specimen after solution treatment yet before tension, showing annealing twins and steps several microns high on the annealing twin boundaries.

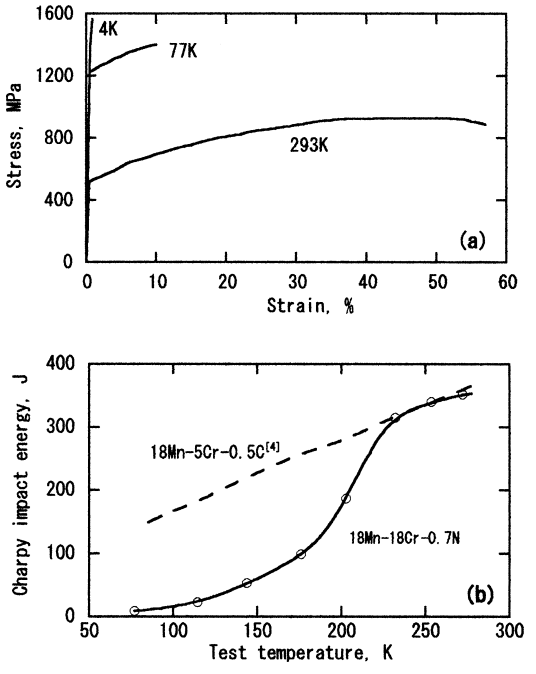

Figure 2 (a) Stress-strain curves and (b) impact energy-temperature curves.

For comparison, the absorbed energy of 18Mn-5Cr-0.5C austenitic steel in Charpy impact tests [4], a typical absorbed energy-temperature curve of austenitic steel, is also shown in Fig. 2b. At 293 K, the test steel exhibits an excellent strength-toughness balance. However, with the decrease in test temperature, the strength of the steel increases significantly, while the elongation and absorbed energy decreased rapidly. It can be seen clearly that the high-nitrogen bearing austenitic steel used in this study obviously presents embrittlement behavior at low temperatures and the ductile-to-brittle transition temperature is about 200 K.

The transition from ductile to brittle behavior of the high-nitrogen austenitic steel can also be seen from the fracture appearance. The SEM fractographs of specimens ruptured at different temperatures are shown in Fig. 3. At room temperature, the steel shows a ductile fracture surface of dimples (Fig. 3a). At lower temperatures, however, the fracture surface becomes to brittle fracture surface consisting of facets of different morphologies. The sizes of the facets are about the same as the sizes of the austenite grains (Fig. 3b and c). The facet F_1, surrounded with dashed lines in Fig. 3b, is flat and smooth. The facet F_2 framed with broken lines in Fig. 3c contains three flat and smooth subfacets f_1, f_2, and f_3 and three rough subfacets f_4, f_5, and f_6. f_1 and f_2 correspond to an annealing twin boundary respectively and f_4 and f_5 correspond to an annealing twin and the matrix respectively (as will be seen from Fig. 5, an SEM photo taken by a simultaneous bi-surface observation technique), while f_5 and f_6 are connected together with f_3 enveloped between them. Hence, facet F_2 corresponds to a coarse austenite grain. Facets F_1 and F_2 are quite the same as the so-called transgranular cleavage-like fracture facets reported by Tobler and Meyn [1] in an 18Cr-3Ni-13Mn-0.37N austenitic steel and by Tomota *et al.* [2, 4] in an 18Cr-18Mn-0.5N austenitic

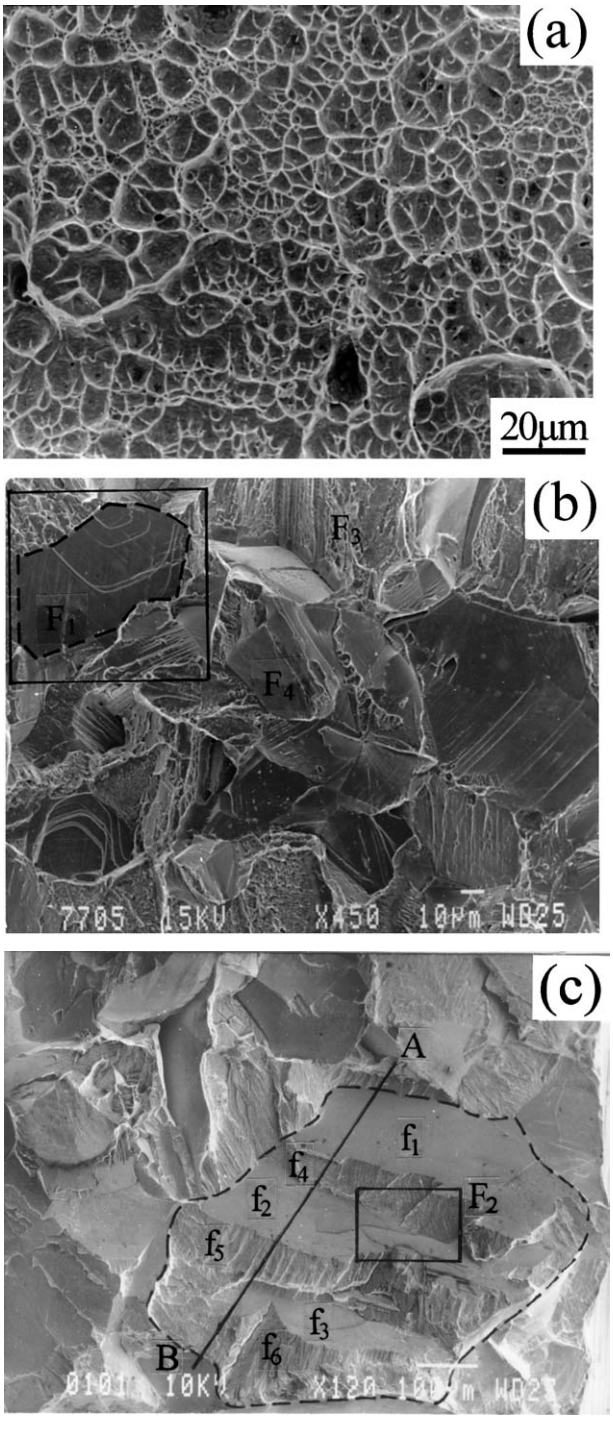

Figure 3 SEM fractographs for specimens: (a) impact fractured at 293 K, (b) impact fractured at 77 K, and (c) tensile fractured at 4 K.

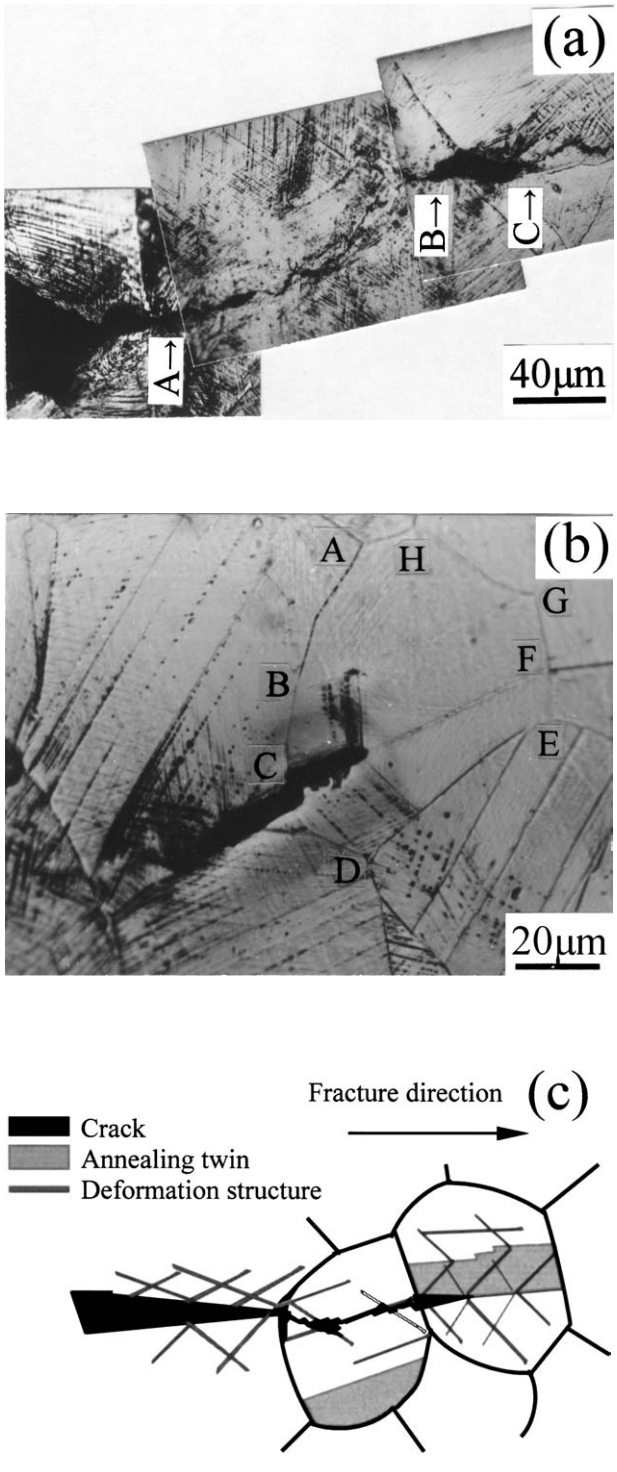

Figure 4 Fracture path at low temperature: (a) crack along a grain boundary and through a grain in a partially ruptured specimen, (b) microcrack ahead of the main crack in a partially ruptured specimen, and (c) schematic illustration of the crack propagation process at low temperature.

steel. It should be noticed that the facet F_1 in Fig. 3b and the facet F_2 in Fig. 3c exhibit some of the characteristics of cracking along special crystallographic plane, but there are not any river pattern on them.

3.3. Relationship between crack propagation paths and fracture facets

In order to clarify the nature of the fracture facets at low temperatures, Charpy specimens were partially ruptured with reduced impact load at 77 K. The microstructure and fracture path near the crack tip were examined by optical microscope from the side surface of the specimen after grinding, polishing, and etching. The results are shown in Fig. 4. In Fig. 4a, a main crack propagates from left to right and comes to point C. It extends through an austenite grain from A to B, and then along grain boundary from B to C. The intergranular crack from B to C is much wider in the direction perpendicular to the crack propagation direction than the transgranular crack from A to B, indicating that the former formed prior to the latter during the crack propagation. In Fig. 4b, a microcrack is observed in front of the main crack in another specimen. Compared with Fig. 1, it

can be seen that ABCDEFGHA in Fig. 4b represents an austenite grain with annealing twin BCFGB and annealing twin boundaries BG and CF in it. The microcrack in the left side is formed along grain boundary while the microcrack in the right side is formed along the annealing twin boundary CF. Around the microcrack, there are a large number of black lines resulting from deformation (hereafter called planar deformation structure). This kind of microcrack can often be observed in front of the main crack in partially ruptured specimens, and they are usually formed along grain boundaries and annealing twin boundaries. Crack propagation goes on by merging the microcrack into the main crack, usually via transgranular fracture, as schematically illustrated in Fig. 4c. In this figure, AB denotes the main crack spreading from left to right, CD the microcrack formed along grain boundary or annealing twin boundary ahead of the main crack, and BC the transgranular crack by which AB and CD are joined. It is now clear that three kinds of fracture modes, annealing twin boundary cracking, intergranular cracking, and transgranular cracking, exist in the low temperature brittle fracture of the steel. It also shows that grain boundary and annealing twin boundary are preferential locations where the crack initiates.

To establish the relationship between fracture paths and fracture facets and make clear the essence of the complex fracture patterns, the fracture surface and the adjacent side surface were examined by a simultaneous observation technique using an SEM. The opposite part of the fractured specimen in Fig. 3c was embedded with resin by impregnated the specimen with resin in a plastic mold, and then sectioned perpendicularly to the macroscopic surface along line AB in Fig. 3c. After the sectioned side surface was polished and etched, the resin was removed from the specimen. The microstructure on the side surface was observed together with the subfacets and the large steps on the fracture surface. The result was shown by an SEM photograph in Fig. 5. The broken line A′B′ in Fig. 5 corresponds to line AB in Fig. 3c. The part above A′B′ shows the fracture surface and the part under A′B′ shows the microstructure on the side surface. In Fig. 5, f_1', f_2' correspond to f_1, f_2 in Fig. 3c and f_4', f_5' in Fig. 5 correspond to f_4, f_5 in Fig. 3c, respectively. Thus it can be seen clearly that the flat subfacets were induced by fracture along annealing twin boundaries, while the rough subfacets resulted from fracture through twin grains, i.e., from transgranular fracture. The above analysis indicates that the flat facets in low temperature brittle fracture (for example, F_1 in Fig. 3b, f_1, f_2, and f_3 in Fig. 3c) are formed by annealing twin boundary cracking, and the rougher facets (for example, F_3 in Fig. 3b, f_4, f_5 and f_6 in Fig. 3c) are induced by transgranular fracture. In addition, it is also confirmed by the bi-surface observation that the smooth curved facet (for example, F_4 in Fig. 3b) is induced by intergranular cracking.

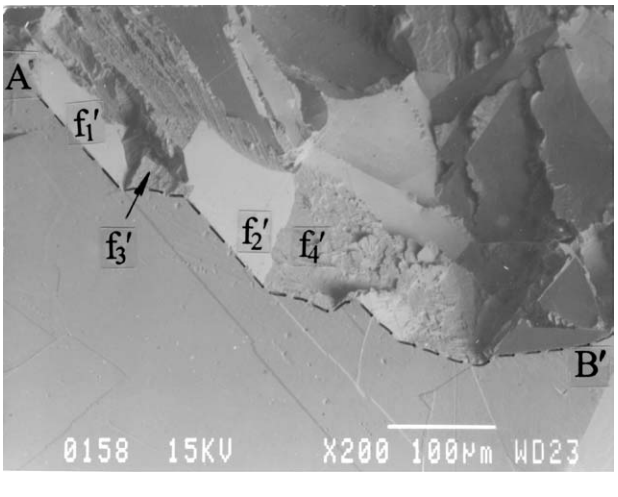

Figure 5 SEM micrograph of dual-plane observation of fracture surface and microstructure of the side surface for specimen fractured at 4 K.

Using this technique, three kinds of fracture modes, namely annealing twin boundary cracking, intergranular cracking and transgranular cracking, are identified in the low temperature brittle fracture of high-nitrogen bearing austenitic steel. We present hereafter the detailed observations on the annealing twin boundary cracking. The other two kinds of fractures will be discussed in the future papers.

3.4. Characteristics and formation of the facet of annealing twin boundary cracking

3.4.1. Characteristics of the facet on annealing twin boundary fracture

The typical feature of the facet of annealing twin boundary cracking is its flatness and smoothness. In addition, there is a pattern of three sets of parallel straight-lines that intersect each other at 60°, bent steps, intrusions, and extrusions on the facet.

Fig. 6a shows an enlarged SEM photograph for the framed area in Fig. 3c. It has already been demonstrated in the above section that the flat facets in Fig. 3c are annealing twin boundary fracture facets. Since the twin boundaries lie in an {111} planes, the annealing twin boundary facets are naturally {111} planes. A pattern of three sets of parallel straight-lines exists on the facet (denoted by dashed lines in Fig. 6a) and the included angles between these three sets of parallel straight-lines are 58°, 60°, and 62° respectively. The facet possesses, to all appearance, all of the features of the transgranular cleavage-like facets reported in the earlier works [1]. In those works, the facets were identified as {111} planes by means of trace analysis [1], etching pit analysis [4, 11], and X-ray diffraction [1] techniques. It was also identified in the early works that planar deformation structures form along {111} planes in the process of low temperature brittle fracture of high-nitrogen austenitic steels, and the straight-line pattern on the fracture surface is just a product of the interactions of the planar deformation structures with the fracture facets [1–4]. Moreover, several steps denoted by arrows in Fig. 6a can be seen on the facet, where segments AA and BB are parallel to each other, and parallel to one set of the straight-lines, i.e., one set of {111} planes.

Fig. 6b shows another SEM photograph of the planar facet for specimen impact ruptured at 77 K (enlarged photograph of the rectangle in Fig. 3b). There are four sets of {111} planes in fcc lattice. If a fracture facet

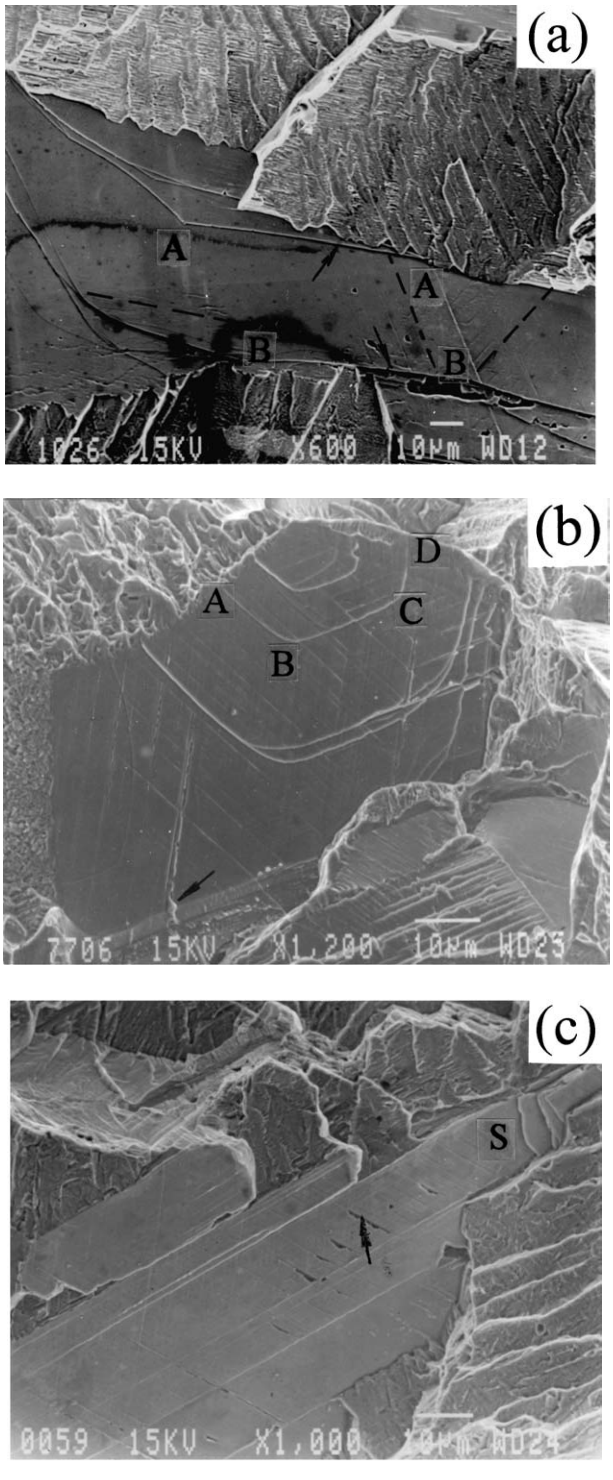

Figure 6 SEM fractographs of annealing twin boundary fracture facets for Charpy specimens fractured at 77 K. (a) and (b) are enlarged micrographs of the framed areas in Fig. 2 (c) and (b) respectively. (c) annealing twin boundary fracture facet with extrusions.

is one of the four sets of {111} planes, the planar deformation proceeding on the other three sets of {111} planes will form a pattern of three sets of straight-lines intersected at 60° on the facet. In practice, however, plastic deformation will occur and induce distortion in the fracture process. And moreover, the incident electron beam in the SEM may not be exactly perpendicular to the fracture facet. Thus the angles measured on the facet may have certain deviation from 60°. The angles of the intersections in Fig. 6b are 58°, 60°, and 62° respectively, similar to those observed in the earlier work [1] and the values in Fig. 6a. Therefore, it is reasonable to consider the facet in Fig. 6b to be formed along {111} planes. Like the steps on the facet of annealing twin boundary in Fig. 6a, a series of steps appear on the facet in Fig. 6b. One of the steps is denoted by ABCD and can be described as bent step when the magnification is not large enough. For the bent step ABCD, AB, BC and CD are all straight, parallel to one set of the straight-lines, i.e., one set of {111} planes, respectively, showing a definite crystallographic feature. The straight segments in ABCD are connected one another by smooth curve. The bent steps do not form a closed loop. They originate from one part of a grain boundary, extend or bend on the facet, and then end up at another part of the grain boundary. These steps are different from the deformation structures that intersect at acute angles instead of smooth bend.

Fig. 1 shows the appearance of steps on annealing twin boundaries on a two dimensional surface of the steel tested. The height of the steps corresponds to that of the steps on the facet of annealing twin boundary fracture. By continual polishing and observation, it was found that the steps on the annealing twin boundaries are bent in the three dimensional space. Weatherly [12] demonstrated, in his research work on the structure of Mg_2Si ledges (another expression for steps) in Al-1.5 wt% Mg_2Si alloy, that the precipitation of Mg_2Si phase is in the form of ledges. The morphology of Mg_2Si precipitate ledges is bent, but not a closed loop. Each of the ledge segments has its own specific crystallographic features when the ledge-matrix interface is coherent or semi-coherent. It is most possible that the steps on the annealing twin boundaries of the steel tested are similar to those Mg_2Si ledges discussed by Weatherly [12] and to the bent step ABCD on the facet of the annealing twin fracture in Fig. 6b.

Beachem *et al.* [13] have revealed the topological features of grains formed during solidification by observing the intergranular facets. It is thus reasonable to believe that the steps on the facets of annealing twin boundaries in Fig. 6a and b are a natural reflection of the geometrical features of annealing twin boundary. On the other hand, the existence of these steps gives a strong evidence that the facet is the product of annealing twin boundary cracking, not just a {111} plane cracking.

In the same light, the facet in Fig. 6c is also considered as a facet of annealing twin boundary cracking since three sets of straight-lines intersecting at about 60° and steps (denoted by s) are present on the facet.

In addition, intrusion and extrusion are seen on the facets, as shown by arrows in Fig. 6b and c, respectively. They are similar to the tongues on the cleavage facet in bcc materials. They are proposed to be produced by a local transgranular cracking on either side of the annealing twin boundary.

3.4.2. Formation of the facets on annealing twin boundary fracture

The microstructure observation revealed that there are a lot of annealing twins in the solution treated specimens

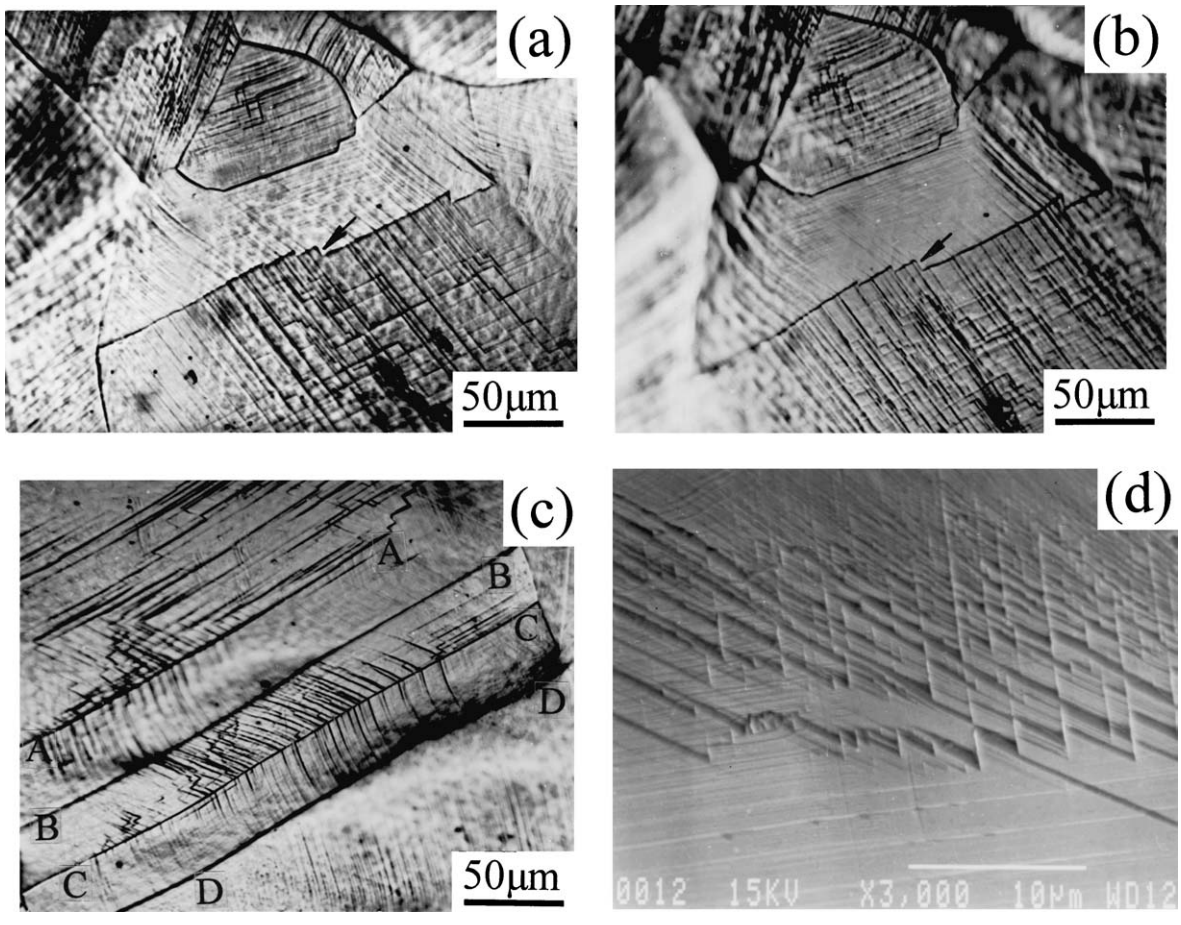

Figure 7 Microstructure changes after deformation and reliefs on annealing twin boundary fracture facet: (a) optical microstructure of a tension specimen subjected to 6% elongation at 293 K. Picture was taken at the same site as in Fig. 1, (b) *in-situ* optical microstructure of the same specimen as in Fig. 7a subjected to 13% elongation at 293 K, (c) optical microstructure of a tension specimen subjected to 13% elongation at 293 K, and (d) SEM photograph of reliefs on an annealing twin boundary fracture facet on a Charpy specimen fractured at 77 K.

of the steel. On the annealing twin boundaries there are many steps a couple of microns high as shown in Fig. 1. Under tensile or impact load, there will also be deformation structure. The formation of deformation structure and its interaction with annealing twin boundary was observed *in-situ*. The specimen showing the microstructure in Fig. 1 was loaded in tension at 293 K until 6% elongation was reached. Its microstructure at the same site as in Fig. 1 is shown in Fig. 7a after unloading. Then, reloaded the specimen till 13% elongation was reached. Microstructure at the same site was taken again after unloading and is shown in Fig. 7b. It is easy to see that a large number of parallel planar deformation structures formed on the original solution-treated microstructure, and the amount of the deformation structures increases as the amount of deformation of the specimen increases. Still, the deformation structures of different orientations in the crystal intersect one another. Crystals on the both sides of a grain boundary or an annealing twin boundary orient differently, so do the deformation structures. Fig. 7c shows the result of *in-situ* observation for another tensile specimen. Based on the observation prior to tension, it was known that lines AA, BB, CC and DD in Fig. 7c are all annealing twin boundaries, and the adjacent linear structures are all formed during deformation. From Fig. 7c, it can be seen that the deformation structures are blocked by the annealing twin boundaries and stress concentration would arise as a consequence. According to Fig. 7a, it can be known that the higher step (denoted by the arrow) parallels approximately to a set of deformation structures, i.e., a set of {111} planes. Comparing with Fig. 1, it is known that this step was formed during solution annealing, not being deformation structure. Generally, annealing twin boundaries are coherent boundaries. Thus the steps on the annealing twin boundaries are incoherent. This indicates that the steps on the annealing twin boundaries show some crystallographic orientations although they are incoherent.

Microstructure of the high nitrogen bearing austenite steel after low temperature deformation is narrow and straight under SEM and metallograph. Literature [1] termed this kind of microstructure "slip-lines". However, literature [2] called it "planar lines," and literature [4] called it "linear markings". There are also transmission electron micrograph (TEM) observations reported in several works to investigate the deformation structures. But unfortunately, the results show some differences. Müllner *et al.* [6] believed that the deformation structures are basically deformation twins. Tomota *et al.* [4] detected planar dislocations and dislocation bands, but neither twin nor martensite was observed. Liu *et al.* [10] found planar slip bands and stacking faults. In the present paper, the emphasis was focused upon the characteristics and formation of the fracture facets, not including detailed work on deformation

structure. In accordance to the above literatures, planar deformation structure is used for the low temperature deformation structure in this study.

On the facets of annealing twin boundary fracture, reliefs with specific crystallographic features can also be seen at higher magnification. Fig. 7d shows a facet fractured at 77 K. This facet is smooth and flat, and there appear three sets of parallel planar deformation structures that intersect one another at approximate 60° on the facet, showing the features of the facet of annealing twin boundary fracture. It should also be noticed that there are many reliefs on the facet. They show obvious crystallographic features and are formed by slipping of three sets of planar deformation structures into or out the facet of annealing twin boundary fracture.

Based on the observations discussed above, a model, schematically shown in Fig. 8, is proposed to illustrate the mechanism of annealing twin boundary cracking.

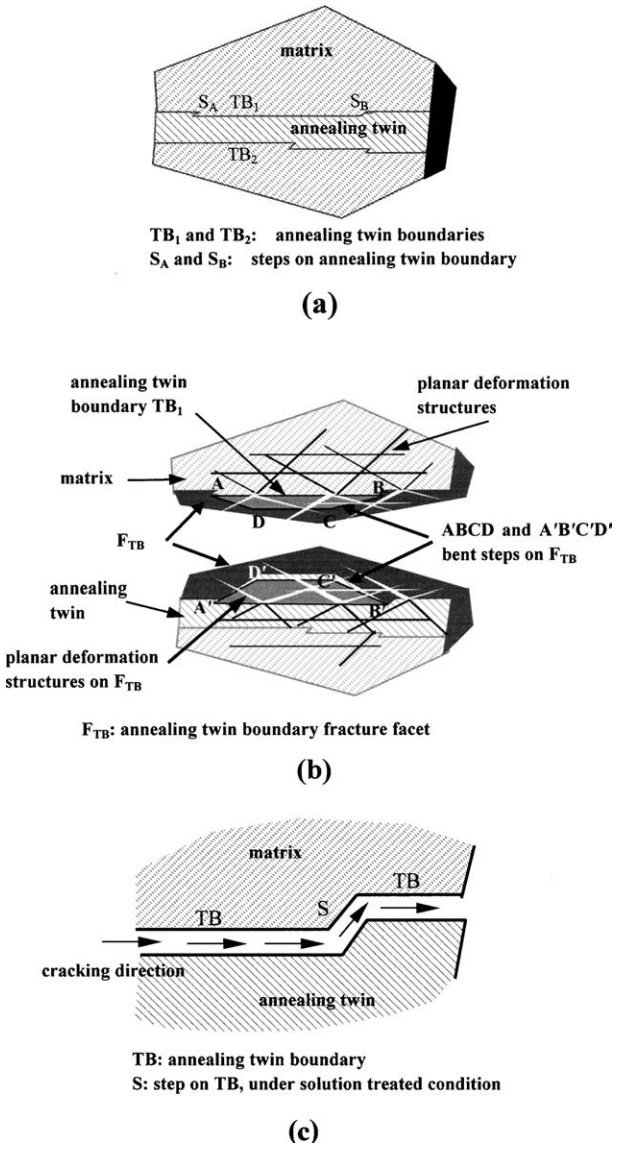

Figure 8 Schematic illustration of annealing twin boundary crack: (a) schematic structure on a section of an austenite grain after solution treatment. There are steps on the annealing twin boundaries, (b) bi-surface views of the fracture along annealing twin boundary TB_1 in Fig. 8a and the structure on the original section, and (c) crack changes its direction of propagation when it meets the step on annealing twin boundary, forming a step on the fracture facet.

In Fig. 8a is a schematic structure on a section of an austenite grain after solution treatment, which includes the matrix, annealing twin and steps on the annealing twin boundaries TB_1 and TB_2 (e.g., steps S_A and S_B on TB_1). Fig. 8b is a schematic drawing showing the bi-surface views of the fracture along annealing twin boundary TB_1 in Fig. 8a and the structure on the section. Compared with Fig. 8a, the planar deformation structures formed along activated {111} planes appear in the structure on the section in Fig. 8b, and they intersect the annealing twin boundary. The discontinuity of the planar deformation structures at the annealing twin boundary causes stress concentration at the intersections of the planar deformation structures with the annealing twin boundary and microcracks are initiated. Eventually, a large number of microcracks connect together and the annealing twin boundary fracture occurs, resulting in two annealing twin boundary fracture facets (as denoted by F_{TB} in Fig. 8b). Planar deformation structures slip out the annealing twin boundary, forming straight-line patterns on the annealing twin boundary fracture facet. The crack propagating along an annealing twin boundary will change its direction of growth when meeting a step of annealing twin boundary, and will propagate along the step of the annealing twin boundary. At the other end of the step, it will propagate in its original direction again along the annealing twin boundary, but at another level (Fig. 8c). Thus, a step on the facet is formed. As mentioned above, steps on annealing twin boundaries are bent. Hence, the steps formed on the fracture facets are bent too, as shown by ABCD and A′B′C′D′ on fracture facet F_{TB} in Fig. 8b. The existence of this kind of step leads to the conclusion that the flat and smooth facets result from annealing twin boundary cracking, not from the transgranular cleavage-like fracturing. When the stress condition is favorable, local transgranular cracking on either side of the annealing twin boundary will occur which results in the extrusions and intrusions on the fracture facet.

The causes why temperature induces a change in fracture mode of high nitrogen steels have been investigated to some extent in previous papers. As temperature decreases, the yield strength of high nitrogen steels increases greatly, and the fracture mode changes [1, 4]. As for the causes of the increment in yield strength, Tomota *et al.* [4] believed that it results from strengthening by short range ordering of nitrogen atoms. Liu *et al.* [10] considered that low stacking fault energy and low temperature planar slip may be the possible causes. However, further research work is still needed to clarify the causes of the change in fracture mode at low temperatures.

4. Conclusion

(1) Crack path and bi-surface observations indicate that the high nitrogen bearing austenitic steel used in this study shows a clear ductile-to-brittle transition behavior. Three kinds of fracture modes at low temperatures, namely annealing twin boundary cracking, intergranular cracking, and transgranular cracking, have been identified.

(2) There are a lot of annealing twins in the steel after solution treatment. On the annealing twin boundaries, there are steps that are several microns high and bent in space. In the brittle fracture process at low temperatures, planar deformation structures are formed on activated {111} slip planes. Annealing twin boundary cracking is induced by interaction of the planar deformation structures with the annealing twin boundaries. Thus formed fracture facets are flat and smooth, with typical features such as bent steps, the pattern of three sets of straight-lines intersecting at 60°, extrusions, and intrusions etc. The bent steps on the facets result from partial propagation of crack along steps that are developed on annealing twin boundaries during solution treatment. The pattern of three sets of parallel straight-lines intersecting at 60° is induced by interaction of the planar deformation structures with the fracture facet. The extrusions and intrusions are results of local transgranular cracking on either side of the annealing twin boundaries.

Acknowledgement

The authors thank the Japan Steel Works Ltd. for supplying the experimental steel.

References

1. R. L. TOBLER and D. MEYN, *Metall. Trans.* A **19A** (1988) 1626.
2. Y. TOMOTA and S. ENDO, *Iron Steel Inst. Jpn. Int.* **30** (1990) 656.
3. C. KANGMIN and D. QIXUN, *J. Iron Steel Res.* **10**(1) (1998) 38 (in Chinese).
4. Y. TOMOTA, Y. XIA and K. INOUE, *Acta Mater.* **46** (1998) 1577.
5. ASTM Designation E616-82, "1987 Annual Book of ASTM Standards," Vol. 03.01 (ASTM, Philadelphia, PA, 1987) Sec. 3, p. 859.
6. P. MÜLLNER, C. SOLLENTHALER, P. J. UGGOWITZER and M. O. SPEIDEL, *Acta Metall. Mater.* **42** (1994) 2211.
7. I. L. MAY, "Principles of Mechanical Metallurgy," (Edward Arnold, Ltd., London, 1981) p. 241.
8. H. LIEBOWITZ, "Fracture: An Advanced Treatise," Vol.1 (Academic Press, New York, 1968) p. 299.
9. M. A. MEYERS, "Mechanical Metallurgy" (Prentice-Hall, Inc., New Jersey, 1984) p. 645.
10. S. LIU, T. HASHIDA, H. TAKAHASHI, H. KUWANO and Y. HAMAGUCHI, *Metall. Trans.* A **29A** (1998) 791.
11. K. SHIBATA and T. FUJITA, *Tetsu-to-Hagané* **71** (1985) S601.
12. G. C. WEATHERLY, *Acta Metallurgica.* **19** (1971) 181.
13. C. D. BEACHEM and R. M. N. PELLOUX, "Fracture Toughness Testing and Its Applications," A Symposium Presented at the Sixty-Seventh Annual Meeting of American Society for Testing and Materials (American Society for Testing and Materials, PA, 1964) p. 210.

Received 13 November 2002
and accepted 14 January 2004